Article

Cell Reports

The Role of Type VI Secretion System Effectors in Target Cell Lysis and Subsequent Horizontal Gene Transfer

Graphical Abstract

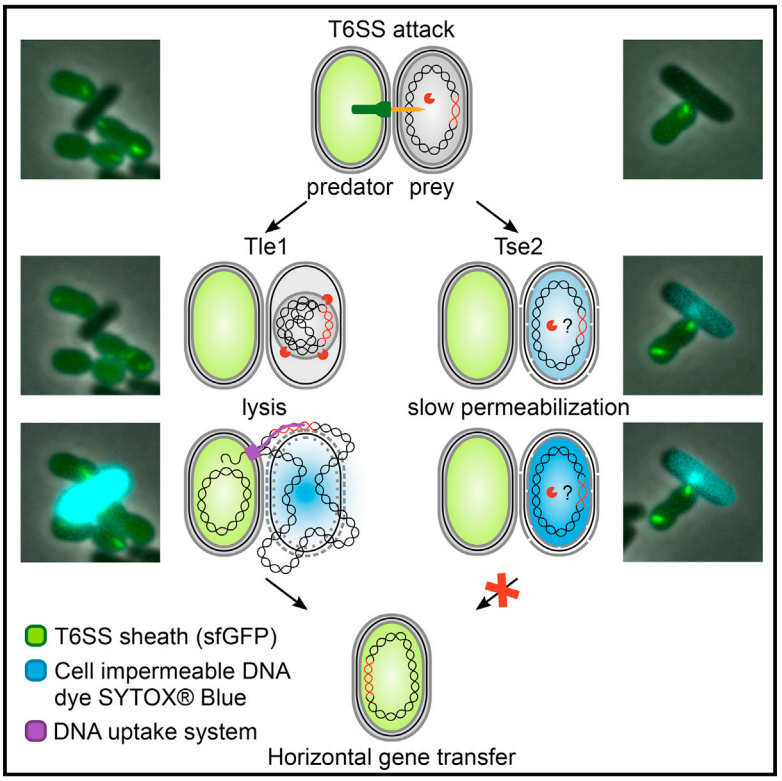

Highlights

- *Acinetobacter baylyi* assembles a dynamic antibacterial type VI secretion system
- Killing and lysis of prey bacteria differs for each of the five effectors
- Gene transfer from prey to predator depends on delivery of lytic effectors

Authors

Peter David Ringel, Di Hu, Marek Basler

Correspondence

marek.basler@unibas.ch

In Brief

Ringel et al. show that naturally competent *Acinetobacter baylyi* ADP1 uses its type VI secretion system to kill bacterial competition by delivery of five different effectors. Lysis of prey cells induced by delivery of lytic effectors is required for efficient transfer of DNA from prey to predator.

Ringel et al., 2017, Cell Reports *21*, 3927–3940
December 26, 2017
https://doi.org/10.1016/j.celrep.2017.12.020

CellPress

Cell Reports
Article

The Role of Type VI Secretion System Effectors in Target Cell Lysis and Subsequent Horizontal Gene Transfer

Peter David Ringel,[1] Di Hu,[1,2] and Marek Basler[1,3,*]
[1]Focal Area Infection Biology, Biozentrum, University of Basel, Klingelbergstrasse 50/70, CH-4056 Basel, Switzerland
[2]Present address: GE Healthcare Shanghai, No. 1 Huatuo Road, Pudong New District, Shanghai, China
[3]Lead Contact
*Correspondence: marek.basler@unibas.ch
https://doi.org/10.1016/j.celrep.2017.12.020

SUMMARY

Bacteria use type VI secretion systems (T6SSs) to manipulate host cells during pathogenesis or to kill competing bacteria, which, in some cases, increases horizontal gene transfer. These functions largely depend on T6SS regulation, dynamics, and the set of effectors that the system delivers into the target cells. Here, we show that *Acinetobacter baylyi* ADP1 assembles a highly dynamic T6SS capable of killing and lysing bacterial cells. T6SS function depends on conserved T6SS components as well as *Acinetobacter*-specific genes of unknown function. Five different effectors, encoded next to VgrG or PAAR proteins and their cognate immunity proteins, cause distinct changes in the prey cells, resulting in various degrees of their lysis. Prey lysis correlates with the rate of DNA transfer from prey to predator, suggesting that lytic effectors are required for efficient T6SS-dependent horizontal gene transfer in naturally competent bacteria.

INTRODUCTION

Bacteria secrete various substrates by specialized secretion systems to manipulate their environment (Costa et al., 2015). The type VI secretion system (T6SS) (Pukatzki et al., 2006) gene clusters are found in more than 25% of all sequenced Gram-negative bacteria, but mostly in the proteobacteria (Bingle et al., 2008). Systems similar to the proteobacterial T6SS have been discovered in *Francisella* (de Bruin et al., 2007; Clemens et al., 2015), *Bacteroidetes* (Russell et al., 2014a), and more recently in *Amoebophilus asiaticus* (Böck et al., 2017), overall constituting four phylogenetically distinct subgroups.

The T6SS is composed of three distinct substructures: the membrane complex, the baseplate, and the sheath-tube complex (Basler et al., 2012; Chang et al., 2017). The envelope-spanning membrane complex is usually composed of TssJ, TssL, and TssM and anchors the T6SS to the cell envelope (Durand et al., 2015). The baseplate is composed of TssE, TssF, TssG, TssK (Brunet et al., 2015), and, in some organisms, a TssA variant (Planamente et al., 2016). The baseplate serves as a platform for the polymerization of the contractile sheath-tube complex and connects it to the membrane complex. The contractile sheath, consisting of VipA (TssB) and VipB (TssC), forms around the inner tube, which is composed of Hcp (Clemens et al., 2015; Kudryashev et al., 2015; Wang et al., 2017), by adding the sheath subunits at the end that is distal from the baseplate (Vettiger et al., 2017). The initiation of the assembly and the polymerization may require TssA (Zoued et al., 2016). Furthermore, a spike complex is situated at the tip of the Hcp tube, which is composed of a VgrG trimer (Pukatzki et al., 2007) and a PAAR protein (Shneider et al., 2013). The contraction of the sheath is thought to propel the Hcp tube with its associated spike complex into the extracellular medium or the target cell (Basler et al., 2012; Vettiger and Basler, 2016; Wang et al., 2017). The contracted sheath is recycled in an ATP-dependent manner by ClpV or ClpB (Basler and Mekalanos, 2012; Bönemann et al., 2009; Brodmann et al., 2017).

T6SS effectors may constitute extensions of any of the secreted components Hcp, VgrG, or PAAR (Pukatzki et al., 2007; Shneider et al., 2013; Ma et al., 2017), or bind non-covalently to these, then termed "cargo" effectors (Bondage et al., 2016; Hachani et al., 2014; Shneider et al., 2013; Silverman et al., 2013). Some cargo effectors require an adaptor/chaperone protein for secretion, which are not secreted themselves (Liang et al., 2015; Unterweger et al., 2015). To prevent self-intoxication, anti-bacterial effectors are accompanied by cognate immunity proteins, often encoded in close proximity to the corresponding effector (Alcoforado Diniz et al., 2015; Dong et al., 2013; Russell et al., 2014b).

Interestingly, the T6SS of *Vibrio cholerae* is part of the competence regulon, and therefore, killing of target cells may contribute to horizontal gene transfer (Borgeaud et al., 2015). *Acinetobacter baylyi* ADP1 is naturally competent throughout most of its growth (Leong et al., 2017) and encodes a single constitutively active antibacterial T6SS (Basler et al., 2013; Weber et al., 2013). Recently, the combination of natural competence and T6SS-mediated bacterial killing in *A. baylyi* was shown to contribute to the transfer of a plasmid from target cells to the predator, suggesting that this may play a role in the spread of antibiotic resistance in the related *A. baumannii* strains (Cooper et al., 2017).

Here, we characterized the dynamics of the T6SS of *A. baylyi* ADP1 using live-cell fluorescence microscopy and identified and characterized five T6SS effectors and their cognate immunity proteins. We could demonstrate that none of the effectors are

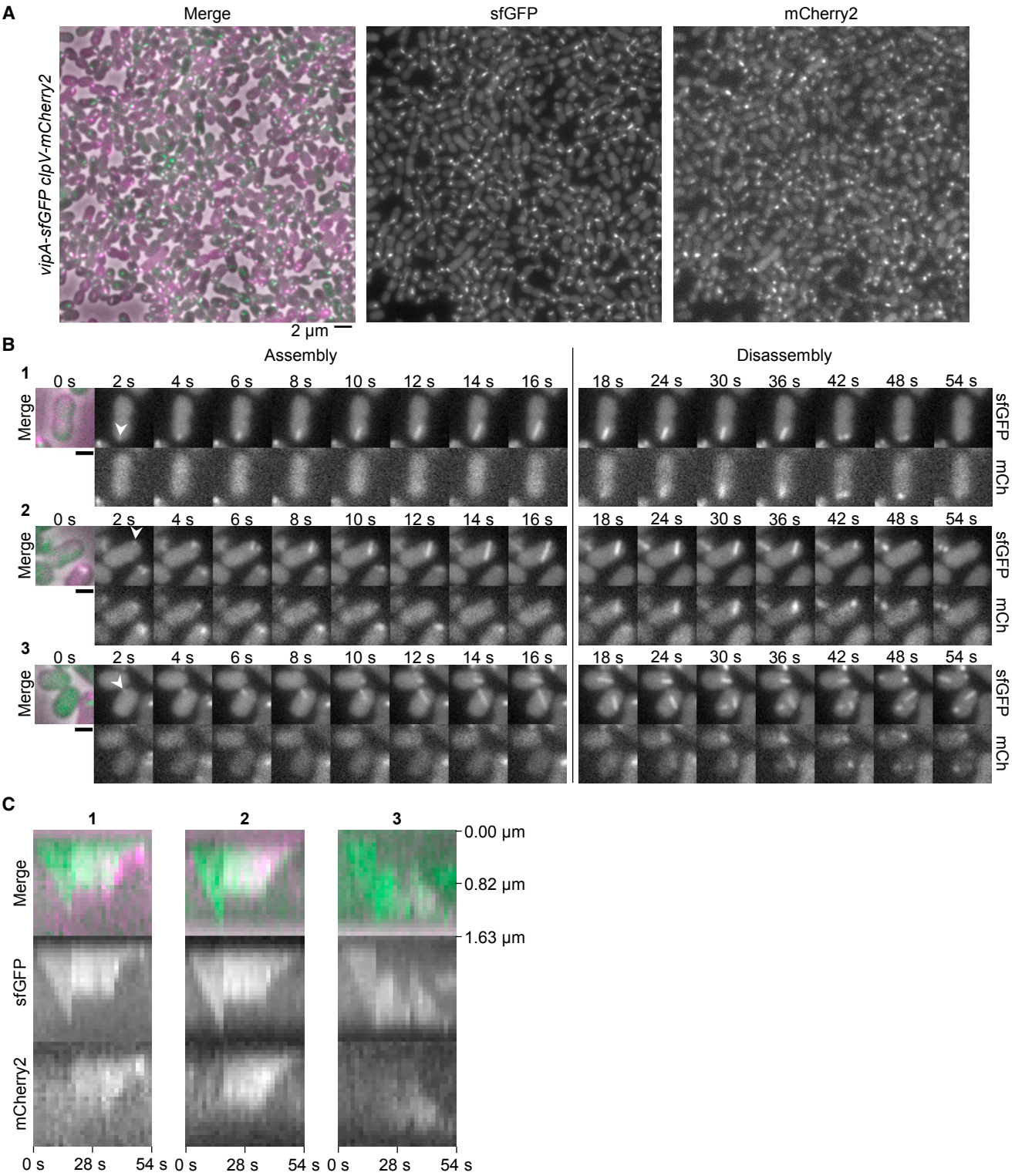

Figure 1. The T6SS Sheath Forms Dynamic Structures in *A. baylyi* ADP1

(A) Large field of view of the parental *A. baylyi* ADP1 *vipA-sfGFP clpV-mCherry2*. The images show: the merge of phase contrast, GFP (in green), and mCherry (in magenta) channels on the left, the GFP channel in the middle, and the mCherry channel on the right.

(B) Three examples of time-lapse imaging of T6SS assembly, contraction, and subsequent disassembly by ClpV. The first frame on the left shows a merge of phase contrast, GFP (in green), and mCherry (in magenta) channels. The frames in the upper rows show fluorescence in the GFP channel (sheath), and the bottom

(legend continued on next page)

required for T6SS assembly and that each kills the target cells by a distinct mechanism. Moreover, we demonstrate that the efficiency of horizontal gene transfer, promoted by the T6SS-mediated lysis of sensitive bacteria, depends on the mechanism of target cell killing.

RESULTS

T6SS Activity in *A. baylyi* ADP1 Correlates with the Formation of Dynamic Sheaths Disassembled by ClpV

To describe the dynamics of the T6SS assembly in ADP1, we first constructed a *vipA-sfGFP* and *clpV-mCherry2* strain, which then served as a parental strain for in-frame deletion mutants unless indicated otherwise (Figure S1A). Live-cell fluorescence microscopy showed that T6SS sheath structures assembled in approximately 15.0 ± 4.2 s (average ± SD, n = 60) and contracted shortly thereafter. Usually, only a single assembling sheath could be observed per cell at any given time. Occasionally, T6SS sheaths polymerized across the whole cell and bent, presumably due to colliding with the cell envelope. On contraction, ClpV-mCherry2 co-localized with the contracted sheath and disassembled it within approximately 40.1 ± 13.4 s (n = 60; Figures 1B and 1C; Movie S2). Importantly, the T6SS activity of the *vipA-sfGFP/clpV-mCherry2* strain was indistinguishable from that of the wild-type strain in its ability to lyse or inhibit growth of *Escherichia coli* as well as secrete Hcp (Figures 2B and 2C), indicating that the fluorescent protein tags have no influence on the T6SS function.

No Hcp could be detected in the supernatant of the Δ*tssM* strain (Figure 2C) and neither the Δ*hcp* nor the Δ*tssM* strains inhibited the growth of *E. coli* or induced its lysis (Figure 2B). Moreover, no dynamic sheath structures were detected in the Δ*tssM* or Δ*hcp* strains (Figure 2A), however, some static VipA-sfGFP foci were observed in the Δ*tssM* strain. This was in contrast to the Δ*tssE* strain, in which we found dynamic VipA-sfGFP foci associated with the cell periphery (Movie S1). Nonetheless, those are unlikely to be functional assemblies, because we were unable to detect Hcp in the supernatant of the Δ*tssE* strain, and the recovery and lysis of *E. coli* were indistinguishable from that of the Δ*tssM* strain (Figures 2B and 2C). We cannot exclude a potential polar effect of the *tssE* deletion on the downstream-encoded TssF and TssG, which were shown to be essential components of T6SS (Brunet et al., 2015; Weber et al., 2016). Although TssE homology to gp25 of the T4 phage suggests its critical role in the assembly and function of T6SS (Kudryashev et al., 2015; Taylor et al., 2016), it was shown for *V. cholerae* that a Δ*tssE* strain retains detectable T6SS activity (Vettiger and Basler, 2016).

TagN, TagF, ACIAD2693, and ACIAD2698 Are Largely Dispensable for T6SS Activity

TagN was proposed to be required for anchoring the T6SS to the peptidoglycan (Aschtgen et al., 2010). In ADP1, the TagN homolog (ACIAD2682) is the only protein encoded in the core cluster bearing a predicted peptidoglycan binding domain and a cleavable N-terminal signal sequence. Surprisingly, the Δ*tagN* strain secreted Hcp and displayed only an intermediate phenotype both in the quantitative competition assay and the lysis assay (Figures 2B and 2C). Furthermore, it had fewer active T6SS structures (Figure 2A; Movie S1). Peptidoglycan was shown to be dispensable for the T6SS activity in *V. cholerae* (Vettiger et al., 2017). However, *V. cholerae* seems to lack T6SS-associated peptidoglycan anchoring proteins (Aschtgen et al., 2010).

Very little is known about the *Acinetobacter*-specific T6SS components ACIAD2693 and ACIAD2698. ACIAD2698 contains a single predicted N-terminal transmembrane helix with the C terminus being disordered and residing in the periplasm. A similar analysis suggested that ACIAD2693 carries a cleavable N-terminal signal sequence and an intrinsically unstructured C-terminal region.

The Δ*ACIAD2698* strain was phenotypically indistinguishable from the parental strain (Figures 2A–2C; Movie S1). On the other hand, the Δ*ACIAD2693* strain secreted Hcp, but displayed an intermediate phenotype in the quantitative *E. coli* competition assay (Figures 2B and 2C). Even though the *E. coli* inhibition was significantly decreased in the absence of ACIAD2693, the lysis of *E. coli* was indistinguishable from that induced by the parental strain (Figure 2B). The decreased inhibition of *E. coli* is in agreement with the reduction in the number of sheath assemblies per cell (Figure 2A). However, the dynamics of the individual T6SS structures were unaltered (Movie S1). Even though *ACIAD2693* overlaps with the essential *vipA*, a polar effect is unlikely the reason for the decreased T6SS activity since the VipA-sfGFP fluorescence was comparable to that of the parental strain (Figure 2A).

TagF was reported to act as a posttranslational repressor of the H1-T6SS in *Pseudomonas aeruginosa* PAO1 (Silverman et al., 2011). However, we observed no change in *E. coli* inhibition or frequency of T6SS sheath assembly in the Δ*tagF* strain. Furthermore, both the lysis of *E. coli* and the Hcp secretion were unaffected (Figures 2A–2C; Movie S1). This suggests that TagF has a different function in *A. baylyi* ADP1 or that it does not act as a repressor under the tested conditions.

TagX and ACIAD2685 Are Required for the Initiation of the T6SS Sheath Assembly

The recently characterized L,D-endopeptidase TagX is thought to be involved in forming a hole in the peptidoglycan, allowing the assembly of the T6SS (Weber et al., 2016). Accordingly, we were unable to detect Hcp in the supernatant of the Δ*tagX* strain, and the *E. coli* inhibition was similar to that caused by the Δ*tssM* strain (Figures 2B and 2C). Interestingly, the more sensitive CPRG conversion assay indicated that the Δ*tagX* strain is still capable of lysing *E. coli*, although to a much lesser extent than the parental strain (Figure 2B), suggesting that the T6SS is still partially active in the absence of TagX. This was

rows show fluorescence in the mCherry channel (ClpV). The arrows indicate the sites where new T6SS sheath structures are forming. The scale bars represent 1 μm.

(C) Kymographs depicting the three examples of assembly, contraction, and subsequent disassembly of the T6SS sheath structures shown in (B). The line for generating the kymogram was drawn along the long axis of the highlighted structure.

See also Movies S1 and S2.

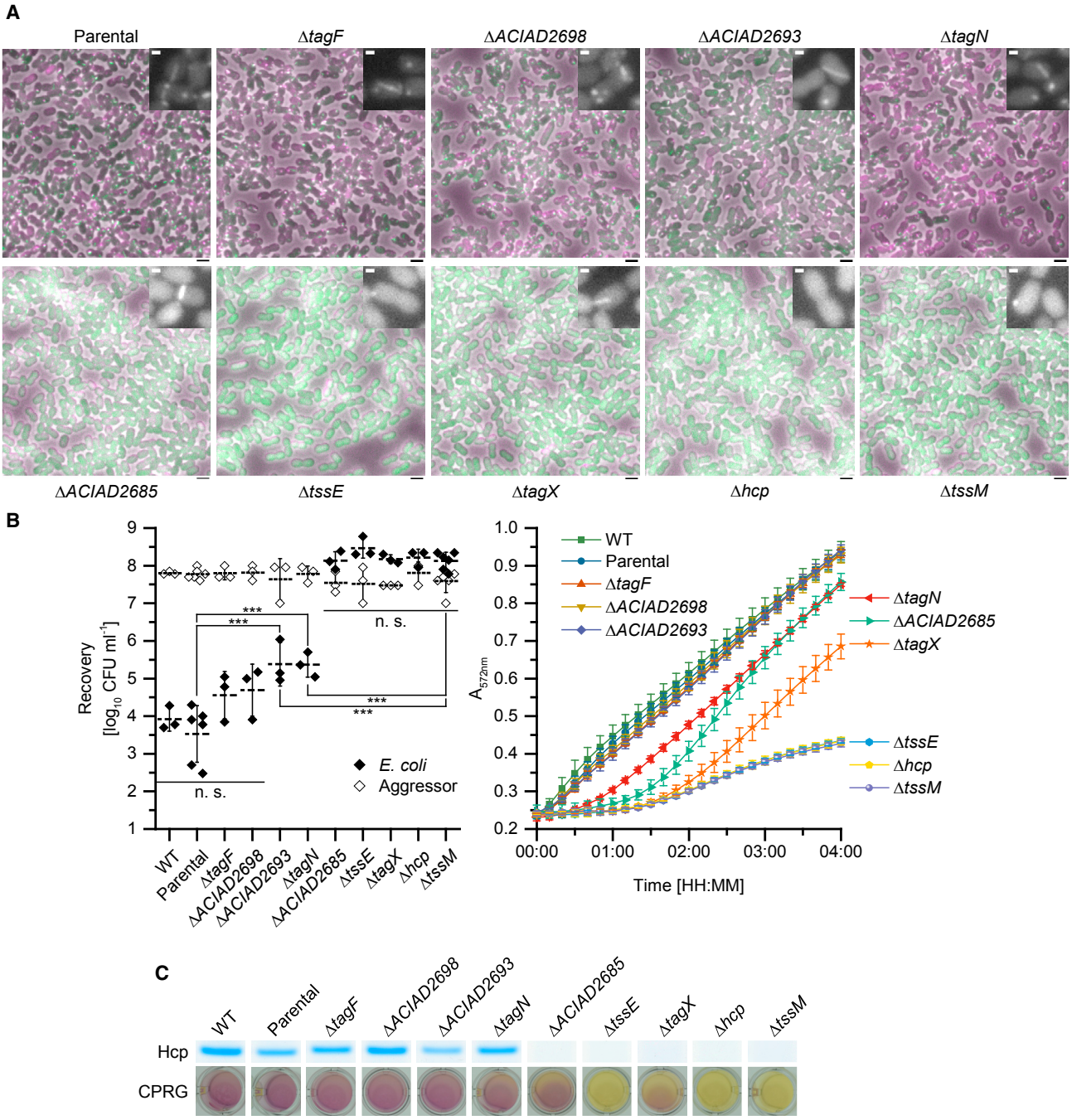

Figure 2. Characterization of Selected T6SS Components of *A. baylyi* ADP1

(A) Large fields of view of the indicated mutants of *A. baylyi* ADP1 showing the merge of phase contrast, GFP (for VipA-sfGFP in green), and mCherry (for ClpV-mCherry2 in magenta) channels. A close up of the GFP channel of a selected region of interest is shown as an inset. The scale bars of the large fields of view represent 2 μm and those of the insets represent 0.5 μm.

(B) The quantitative competition assay measuring recovery of the indicated strains after 4 hr of coincubation of *E. coli* with the indicated aggressor strains is shown on the left. The error bars indicate the SD, the long dashed lines indicate the mean value of the *E. coli* recovery, and the short dashed lines indicate the mean value of the aggressor recovery. n. s. = not significant; ***$p < 0.001$. Lysis assays measuring CPRG conversion upon release of LacZ from *E. coli* cells incubated with the indicated *A. baylyi* strains for the indicated time are shown on the right. The lysis assays were performed in biological triplicate and technical hexaplicate for all competitions except for the parental and the Δ*tssM* strains for which biological and technical hexaplicates were performed.

(C) Hcp detected in the culture supernatant of the indicated strains after trichloroacetic acid (TCA) precipitation, separation by PAGE and subsequent staining with Coomassie. Representative pictures of the endpoints of the lysis assays from (B) are shown for comparison.

See also Figures S1 and S4 as well as Movie S1.

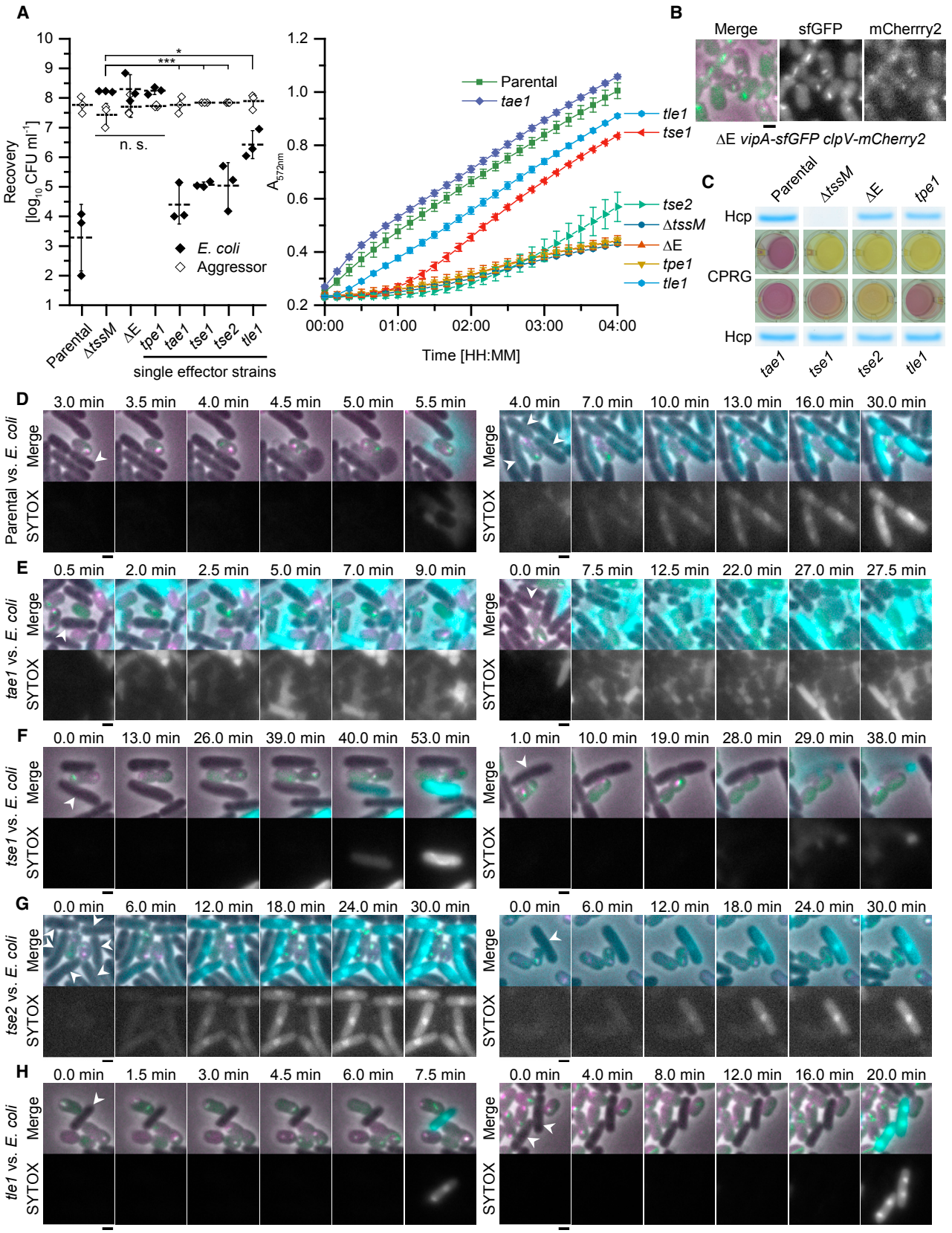

(legend on next page)

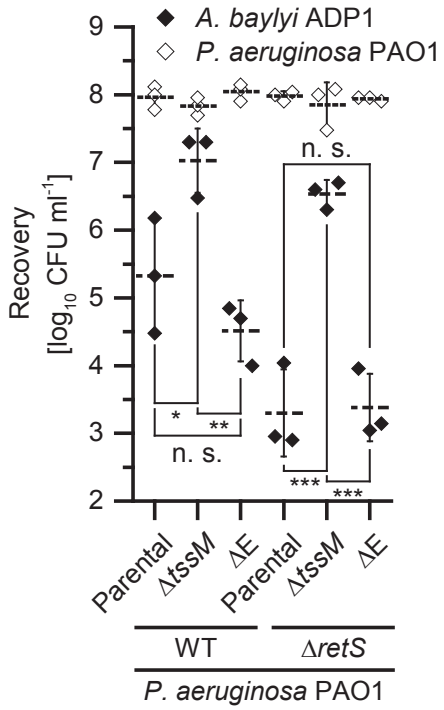

Figure 4. The T6SS Effectors of *A. baylyi* ADP1 Are Dispensable for Eliciting Retaliation from *P. aeruginosa* PAO1

Quantitative competition assays measuring recovery of the indicated *A. baylyi* and *P. aeruginosa* strains upon 4 hr of coincubation. The dashed lines indicate the means and the error bars indicate the SD. n. s. = not significant; *p < 0.05; **p < 0.01; ***p < 0.001.

See also Figure S4.

confirmed by fluorescence microscopy, which revealed a strongly reduced frequency of T6SS sheath assembly initiation (Figure 2A; Movie S1), indicating that TagX is dispensable for the T6SS mode of action after the assembly is initiated by a TagX-independent mechanism.

Bioinformatic analysis of ACIAD2685 suggested the presence of two N-terminal transmembrane helices and that the N- and C-termini are localized in the cytoplasm. The T6SS activity of the Δ*ACIAD2685* strain was severely attenuated. There was no detectable Hcp secretion and no inhibition of *E. coli* (Figures 2B and 2C). However, the more sensitive CPRG conversion assay indicated that *E. coli* lysis was still occurring, albeit to a severely reduced extent (Figure 2B). These results are in agreement with the strongly reduced frequency of T6SS assembly observed by fluorescence microscopy, similar to what had been observed for the Δ*tagX* strain (Figure 2A; Movie S1). TssM is encoded right downstream of ACIAD2685, therefore, we cannot exclude a potential polar effect of the in-frame deletion.

Five Identified T6SS Effectors Are Dispensable for T6SS Dynamics and Hcp Secretion

The fact that T6SS effectors are often found encoded in an operon with a secreted structural component and the cognate immunity protein allowed us to identify five putative effectors and their cognate immunity proteins in *A. baylyi* ADP1 (Figure S1B). An effector-deficient strain (ΔE), lacking all five identified effectors, was still able to secrete Hcp, and its T6SS activity and dynamics, observed by fluorescence microscopy, were unaffected (Figures 3B and 3C; Movie S1). However, we were unable to detect a growth inhibition of *E. coli* or its lysis when competed against the ΔE strain (Figure 3A). Moreover, no *E. coli* permeabilization was detected by fluorescence microscopy using SYTOX Blue as a cell permeability reporter (Movie S3). This suggests that there is no remaining antibacterial effector secreted by the ΔE strain, and that none of the effectors are structural or functional components of the secretion system itself.

To test if the T6SS in the ΔE strain is capable of inflicting damage, we co-incubated the strain with both *P. aeruginosa* PAO1 and its Δ*retS* variant. Interestingly, both the wild-type and the Δ*retS* strain inhibited the *A. baylyi* ΔE strain to the same level as its parental strain. However, the inhibition of *A. baylyi* was significantly reduced when the Δ*tssM* strain was co-incubated with the *P. aeruginosa* wild-type or Δ*retS* strains (Figure 4). This is consistent with previous observations (Basler et al., 2013; Wilton et al., 2016) and suggests that the ΔE strain is likely damaging at least the outer membrane of target cells and thus induces retaliation by *P. aeruginosa*.

Figure 3. *A. baylyi* ADP1 deploys antibacterial T6SS effectors eliciting distinct lysis phenotypes

(A) Quantitative competition assay measuring recovery of the indicated strains after 4 h of coincubation of *E. coli* with the indicated aggressor strains is shown on the left. The error bars indicate the standard deviation, the long dashed lines indicate the means of the *E. coli* recovery and the short dashed lines indicate the means of the aggressor recovery. Lysis assays measuring CPRG conversion upon release of LacZ from *E. coli* cells incubated with the indicated *A. baylyi* strains for the indicated time is shown on the right. The lysis assays were performed in biological triplicate and in at least technical tetraplicate. n. s. = not significant; * = p < 0.05; *** = p < 0.01.

(B) Representative image of effector deficient strain (ΔE *vipA-sfGFP clpV-mCherry2*) shows the merge of phase contrast, GFP (in green) and mCherry (in magenta) channels on the left; the GFP channel in the middle; and mCherry channel on the right. The scale bar is equivalent to 1 μm.

(C) Hcp detected in the culture supernatant of the indicated strains after TCA precipitation, separation by PAGE, and subsequent staining with Coomassie. For comparison, representative images of the endpoints of the lysis assay from (A) are shown.

(D–H) Time-lapse microscopy of the competitions of the parental strain (D) and the *tae1* (E), *tse1* (F), *tse2* (G), and *tle1* (H) single effector *A. baylyi* ADP1 strains with *E. coli*. The representative frames were chosen to illustrate the distinct lysis phenotypes elicited by the indicated effectors. The top rows show a merge of phase contrast, GFP (for VipA-sfGFP in green), mCherry (for ClpV-mCherry2 in magenta), and SYTOX (in cyan) channels. The bottom rows show the increase in the fluorescence of the cell-impermeable DNA stain SYTOX Blue on the loss of cell membrane integrity. The scale bars represent 1 μm. The arrows indicate the cells that lose membrane integrity throughout the time lapse. Except for (F), the competitions were imaged every 30 s for 30 min. For (F), the competitions were imaged every 1 min for 1 hr.

See also Figures S1, S2, and S4 as well as Movies S1 and S3.

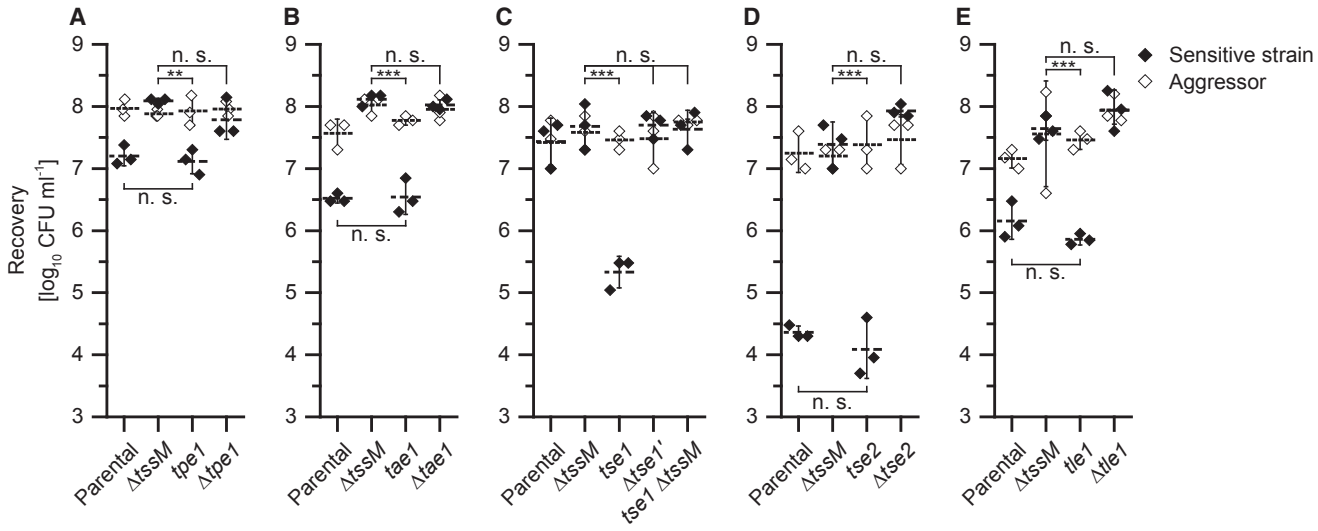

Figure 5. There Is No Crosstalk between the Five T6SS Effectors and Their Cognate Immunity Proteins

(A–E) Quantitative competition assays measuring recovery of the sensitive strains and the specified mutants after 4 hr of coincubation. The error bars indicate the SD, the long dashed lines indicate the mean recovery of the sensitive strains and the short dashed lines indicate the mean recovery of the aggressors. n. s. = not significant; *p < 0.05; **p < 0.01; ***p < 0.001.

(A) Δ*tpe1-tpi1*::*rpsL'-kan*^{R} used as the sensitive strain.

(B) Δ*tae1-tai1*::*rpsL'-kan*^{R} used as the sensitive strain.

(C) Δ*tap1-tsi1b*::*rpsL'-kan*^{R} used as the sensitive strain.

(D) Δ*tse2* Δ*tsi2a-tsi2b*::*rpsL'-kan*^{R} used as the sensitive strain.

(E) Δ*tli1-tle1*::*rpsL'-kan*^{R} used as the sensitive strain.

To investigate the role of the individual effectors, strains lacking all but one of the effectors (single effector strains) were constructed. All five single effector strains secreted Hcp and displayed sheath dynamics similar to the parental strain (Figures 3C–3H; Movie S3). The strains were tested for their ability to lyse or inhibit growth of *E. coli* (Figure 3A). To dissect the mode of action of the individual effectors, we also incubated the strains with *E. coli* and imaged the competition for 30 min to 1 h at 30°C on a Luria-Bertani (LB) agarose pad containing SYTOX Blue as an indicator for cell permeability (Figures 3D–3H; Movie S3). Since putative immunity proteins were identified in the vicinity of the effectors, we constructed strains lacking the immunity-effector pairs and tested their growth inhibition due to interactions with the corresponding single effector, the parental, the single effector deletion, and the Δ*tssM* strains (Figures 5A–5E).

The Putative Metallopeptidase Tpe1 Is a T6SS Effector and Tpi1 Is Its Cognate Immunity Protein

The smallest of the putative effectors, Tpe1 (ACIAD0053), is encoded in an operon with two PAAR proteins (Figure S1B). It is predicted to contain a zinc metallopeptidase active site, PS00142 (Figure S1C). The single effector strain was unable to significantly reduce the recovery of *E. coli* or induce its lysis (Figures 3A and 3C). Additionally, the imaging of the competition with *E. coli* showed no increase in signal from the DNA-binding dye SYTOX Blue, suggesting that no *E. coli* cell permeabilization was occurring (Movie S3).

The protein encoded downstream of Tpe1, which we termed Tpi1 (ACIAD0054), contains a predicted N-terminal transmembrane helix, and we hypothesized it to constitute the cognate immunity protein to Tpe1 (Figure S1B). The competition of the sensitive strain (lacking both Tpe1 and Tpi1) against the parental and the single effector strains led to a significantly reduced recovery of the sensitive strain, whereas there was no such reduction when competed against the Δ*tssM* and the Δ*tpe1* strains (Figure 5A). This indicates that Tpe1 is a T6SS effector and Tpi1 is its corresponding immunity protein. The fact that no *E. coli* inhibition or lysis was detected suggests that either *E. coli* is resistant to the action of Tpe1 or that *E. coli* can outgrow its effects without lysis.

Tae1 Is a Peptidoglycan-Targeting T6SS Effector and Tai1 Is Its Cognate Immunity Protein

The remaining putative T6SS effectors are encoded downstream of VgrGs. Bioinformatic analysis of the sequence of Tae1 (ACIAD0168) suggested that it is a peptidoglycan-hydrolyzing amidase, which has no clear homology to any of the four currently known families (Russell et al., 2012). Tae1 contains two predicted peptidoglycan-binding domains (LysM, PF01476.19, and IPR002477), a D-alanyl-D-alanine carboxypeptidase zinc-binding domain (IPR009045) and a peptidoglycan-hydrolyzing domain (hydrolase_2, PF07486.11; Figure S1C), suggesting that Tae1 cleaves the peptide crosslinks of peptidoglycan. The single effector strain significantly reduced the recovery of *E. coli* and induced its lysis to a level comparable to that of the parental strain (Figures 3A and 3C). Imaging the competition with *E. coli* revealed that lysing *E. coli* often round up and burst (Figure 3E; Movie S3), which is consistent with

the prediction that Tae1 encodes a peptidoglycan-targeting effector.

The gene downstream of *tae1* encodes a protein we termed Tai1 (ACIAD0169), which carries a predicted cleavable N-terminal signal sequence, suggesting that Tai1 is the cognate immunity protein of Tae1. When the Δ*tae1*/Δ*tai1* strain was competed with the parental strain or the Tae1 single effector strain, the recovery of the Δ*tae1*/Δ*tai1* strain was significantly reduced. This was fully dependent on T6SS activity and presence of *tae1*, since the recovery was restored when competed against the Δ*tae1* and the Δ*tssM* strains (Figure 5B). This indicates that Tae1 is a peptidoglycan-targeting T6SS effector and that Tai1 is the cognate immunity protein.

The Restored Tse1 Is a T6SS Effector and Tsi1a or Tsi1b Are Its Cognate Immunity Proteins

Downstream of VgrG2 (ACIAD1788), a protein we termed Tap1 (ACIAD1789) is encoded that shows weak homology to the DUF4123 domain found in T6SS effector chaperones (TECs), also referred to as adaptor proteins (Liang et al., 2015; Unterweger et al., 2015). The downstream gene terminates at a copy of the insertion element IS1236, suggesting that the original gene was disrupted by IS1236 (Figure S1B). Indeed, a BLAST search of the N-terminal fragment Tse1' (ACIAD1790) in the UniParc (The UniProt Consortium, 2017) database yielded longer proteins in various *Acinetobacter* strains, which were in the genomic neighborhood of VgrG and Tap1 homologs and whose N-terminal regions were similar to Tse1'.

We removed the insertion sequence (IS) element and restored the full-length Tse1 based on the multiple sequence alignment with the homologous effectors (ACIAD1790–1794 fusion; Figures S1B and S2). The full-length Tse1 is predicted to carry four C-terminal transmembrane helices and had a low-quality match for the short-chain dehydrogenase/reductase active site (PS00061; Figure S1C). The single effector strain significantly reduced the recovery of *E. coli* and led to intermediate lysis of *E. coli* in the CPRG conversion assay (Figures 3A and 3C). The competition microscopy showed that, in some cases, lysis proceeded similar to what had been observed for Tae1, where *E. coli* rounded up and then burst, whereas in other cases, *E. coli* shrinks slightly and lyses (Figure 3F; Movie S3). Both processes take longer compared with the lysis induced by the other effectors.

Two putative immunity proteins sharing 82% sequence identity are encoded downstream of Tse1, which we termed Tsi1a (ACIAD1795) and Tsi1b (ACIAD1796; Figure S1B). A Tse1 ortholog was only found in *Burkholderia cenocepacia* (excluding *Acinetobacter*), and immunity protein duplications were restricted to *Acinetobacter*, ranging from one to three copies (Figure S3A). Both Tsi1a and Tsi1b are predicted to contain four transmembrane helices. The sensitive strain (lacking both Tsi1a and Tsi1b) was inhibited by the single effector strain carrying the restored Tse1 (Figure 5C). However, no inhibition was observed when competed against the Δ*tssM* strain or the Δ*tse1'* strain as well as the parental strain containing the IS element. When *tssM* was deleted in the single Tse1 effector strain, no reduction in recovery of the sensitive strain could be detected (Figure 5C). This confirms that Tse1 is secreted in a T6SS-dependent manner and that Tsi1a, Tsi1b, or both are the cognate immunity proteins.

Tse2 Is a T6SS Effector and Tsi2a or Tsi2b Are Its Cognate Immunity Proteins

Tse2 (ACIAD3114) is a homolog of the recently described $Tse3_{AB}$ (ACX60_11695) in *A. baumannii* ATCC 17978, which was found to be an antibacterial effector, but its mechanism of action remained unknown (Weber et al., 2016). The single effector strain significantly reduced the recovery of *E. coli*, however, lysis, indicated by the CPRG conversion assay, was delayed compared with the other single effector strains (Figure 3A). Interestingly, *E. coli* only slowly gained SYTOX Blue signal during its interaction with the Tse2 single effector strain, and the signal remained low. This is in contrast to what we observed when *E. coli* was lysed by other effectors (Figure 3G; Movie S3). The slow increase in SYTOX Blue signal suggests that Tse2 leads to a low-level permeabilization of *E. coli*, which is consistent with the delayed conversion of CPRG by LacZ and suggests that the cell envelope remains largely impermeable to CPRG and LacZ.

The two putative immunity proteins Tsi2a (ACIAD3112) and Tsi2b (ACIAD3113), encoded in the opposite direction downstream of the effector (Figure S1B), are predicted to contain a cleavable N-terminal signal sequence, indicating that they are periplasmically localized and suggesting that the subcellular target of Tse2 is accessible from the periplasm. The recovery of the Δ*tsi2a*/Δ*tsi2b*/Δ*tse2*-sensitive strain was significantly reduced after incubation with the parental or the single effector strain, but unchanged when incubated with the Δ*tssM* or Δ*tse2* strains (Figure 5D). These data indicate that Tse2 is a T6SS effector and that Tsi2a, Tsi2b, or both confer immunity toward Tse2.

A manual inspection of gene ortholog neighborhoods of *tse2* revealed the presence of Tse2 homologs mostly in γ-proteobacteria, but also in α- and β-proteobacteria. Multiple copies of the immunity proteins, up to five consecutive ones in *Klebsiella pneumonia* W14 and *Photorhabdus luminescens* subsp. *luminescens* DSM 3368, were a common feature in γ-proteobacteria, but only two duplications were observed for β-proteobacteria, and none were observed for α-proteobacteria (Figure S3B). Immunity protein duplications seem to be common, and all may contribute to immunity (Jiang et al., 2014; Russell et al., 2013; Zhang et al., 2012). These evolved paralogs were speculated to provide immunity against diverged corresponding effectors arising in the population (Kirchberger et al., 2017; Zhang et al., 2012).

The Phospholipase Tle1 Is a T6SS Effector and Tli1 Is Its Cognate Immunity Protein

Tle1 (ACIAD3425) was predicted to be a phospholipase belonging to family 4 of T6SS-associated phospholipases (Russell et al., 2013). It matches an alpha/beta-hydrolase fold (Gene3D 3.40.50.1820) and the abhydrolase_5 domain (PF12695.5; Figure S1C). The Tle1 single effector strain significantly reduced the recovery of *E. coli* and led to intermediate lysis of *E. coli* in the CPRG conversion assay (Figures 3A and 3C). Surprisingly, when the Tle1 single effector strain was co-incubated with *E. coli*, the *E. coli* cells first shrank without an increase of SYTOX Blue signal and then reinflated, coinciding with their permeabilization (Figure 3H; Movie S3).

The putative immunity protein is co-encoded in the same operon upstream of *tle1*, which we termed Tli1 (ACIAD3426). Tli1 carries a predicted cleavable N-terminal signal sequence as is common for the cognate phospholipase immunity proteins (Russell et al., 2013). The recovery of the sensitive strain was significantly reduced when competed against the parental or single effector strain. The recovery was restored when competed against the Δ*tssM* or the Δ*tle1* strains (Figure 5E). These results confirm that Tle1 is a T6SS effector and that Tli1 is its cognate immunity protein.

The T6SS-Mediated Lysis of Prey Contributes to Horizontal Gene Transfer

T6SS-mediated killing of prey cells by the naturally competent *A. baylyi* ADP1 can liberate the DNA of the prey and thereby promote horizontal gene transfer (Cooper et al., 2017). We speculated that effectors causing the release of cellular content, like Tae1 and Tle1, should cause a higher transformation rate than those not directly leading to lysis, like Tse2. To test this hypothesis, we competed a spectinomycin-resistant, T6SS-active *A. baylyi* ADP1 derivative (T6SS$^+$) against the Tle1- and the Tse2-sensitive strains (Figures 6A and 6B). The sensitive strains carry the kanamycin resistance cassette, disrupting the immunity protein-encoding genes. Successful transfer of DNA can thus be monitored by selecting for spectinomycin and kanamycin double-resistant strains.

To account for DNA transfer independent of T6SS-mediated killing, a T6SS-deficient, spectinomycin-resistant strain (T6SS$^-$) was used as a control strain. To exclude possible differences in uptake and integration of the counter-selectable cassettes from the Tle1- and Tse2-sensitive strains, we transformed the T6SS$^+$ strain with equal amounts of the genomic DNA of both sensitive strains and enumerated the resulting double-resistant mutants. The number of transformants obtained with the genomic DNA was not significantly different, indicating that both cassettes incorporate with similar efficiency (Figure 6A).

When we incubated the T6SS$^+$ strain with the Tle1- and Tse2-sensitive strains, we observed reduced recoveries of the sensitive strains comparable with those obtained during our previous assays (compare Figures 5D and 5E with Figure 6B). In addition, similar to the observations made for the competition with *E. coli*, the lipase effector Tle1 induced lysis of the non-immune *A. baylyi* strain (*vipA-sfGFP clpV-mCherry2 Δtli1-tle1*) as documented by the leakage of DNA out of cells, the decrease in contrast of the bacterial cytosol, and the rapid accumulation of SYTOX Blue signal (Figures 6C). On the other hand, the Tse2-effector-mediated killing resulted in a high level of inhibition of the non-immune *A. baylyi* strain (*vipA-sfGFP clpV-mCherry2 Δtse2 Δtsi2a-tsi2b*; Figure 6B), however, no clear cell lysis was observed, and the cells accumulated SYTOX Blue rather slowly (Figure 6D). Importantly, the competition of the T6SS$^+$ strain with the Tle1-sensitive strain produced significantly more double-resistant mutants than the competition of the T6SS$^+$ strain with the Tse2-sensitive strain or the T6SS-independent transfer (Figure 6A). Overall, these data suggest that the mechanisms of killing and lysis of target cells have major implications for DNA release and thus efficiency of horizontal gene transfer.

DISCUSSION

Imaging of *A. baylyi* ADP1 T6SS sheath dynamics and the use of a sensitive target cell lysis assay allowed us to identify *Acinetobacter*-specific T6SS components, which are required for efficient initiation of sheath assembly (Table 1). We predicted and characterized five distinct effectors and their immunity proteins and show that the mechanism of target cell killing influences the efficiency of gene acquisition from prey cells.

We show that a markerless in-frame deletion of *ACIAD2693* only has a partial effect on the T6SS function, and in many assays, the deletion strain displayed a phenotype similar to that of the wild-type *A. baylyi* (Figures 2A–2C; Movie S1). A likely explanation for the discrepancy with the previous results is a potential polar effect on the downstream *vipA* (*tssB*) gene resulting from generating insertion mutants using a Tdk-Kan^R cassette (Weber et al., 2016).

ACIAD2685 and TagX were proposed to be essential for T6SS-mediated Hcp secretion (Weber et al., 2016). Interestingly, we show that the strains lacking ACIAD2685 or TagX occasionally assemble sheath structures that display dynamics similar to that of the parental strain (Figure 2A; Movie S1). Importantly, the prey cell lysis assay shows that those assemblies are functional, which suggests that ACIAD2685 and TagX influence the frequency of T6SS sheath assembly rather than the function of the individual T6SS structures (Figure 2B). This is consistent with the fact that TagX is an L,D-endopeptidase cleaving the peptide crosslinks of the peptidoglycan, which was proposed to form holes in the peptidoglycan to allow assembly of the T6SS (Weber et al., 2016). Similarly, the lytic transglycosylase MltE was recently shown to be recruited by the TssM of the Sci-1 in *E. coli* EAEC 17-2 to fulfil the same purpose (Santin and Cascales, 2017). Therefore, the low number of T6SS assemblies detected in the Δ*tagX* strain may be due to the formation of holes in the peptidoglycan during its remodeling or aging. Although the phenotype of the Δ*ACIAD2685* strain is similar to that of the Δ*tagX* strain, the lack of conserved domains prevents predicting its function.

We identified five T6SS effectors and their corresponding immunity proteins in *A. baylyi* ADP1, a putative metallopeptidase (Tpe1), a peptidoglycan-hydrolyzing amidase (Tae1), a phospholipase (Tle1), and two effectors (Tse1, and Tse2) representing new classes of effectors for which no enzymatic activity could be predicted or deduced from the lysis phenotype. Interestingly, the *A. baylyi* strain lacking all five effectors (ΔE) was unable to inhibit *E. coli* or induce cell membrane leakage (Figures 3A and 3C; Movie S3). This is despite the fact that the ΔE strain assembles dynamic T6SSs secreting wild-type levels of Hcp (Figures 3B and 3C; Movie S1). The ΔE strain also provokes retaliation by *P. aeruginosa* (Figure 4) since it is killed as well as the wild-type *A. baylyi* strain. This suggests that the retaliation from *P. aeruginosa* is independent of effector delivery and is rather a response to membrane perturbations as indicated previously (Basler et al., 2013; Ho et al., 2013; Wilton et al., 2016). Interestingly, this also means that mere puncturing of the target cell membrane is insufficient for killing or lysis of target cells and that the delivery of effector proteins is required. This is consistent with observations that even multiple puncturing of

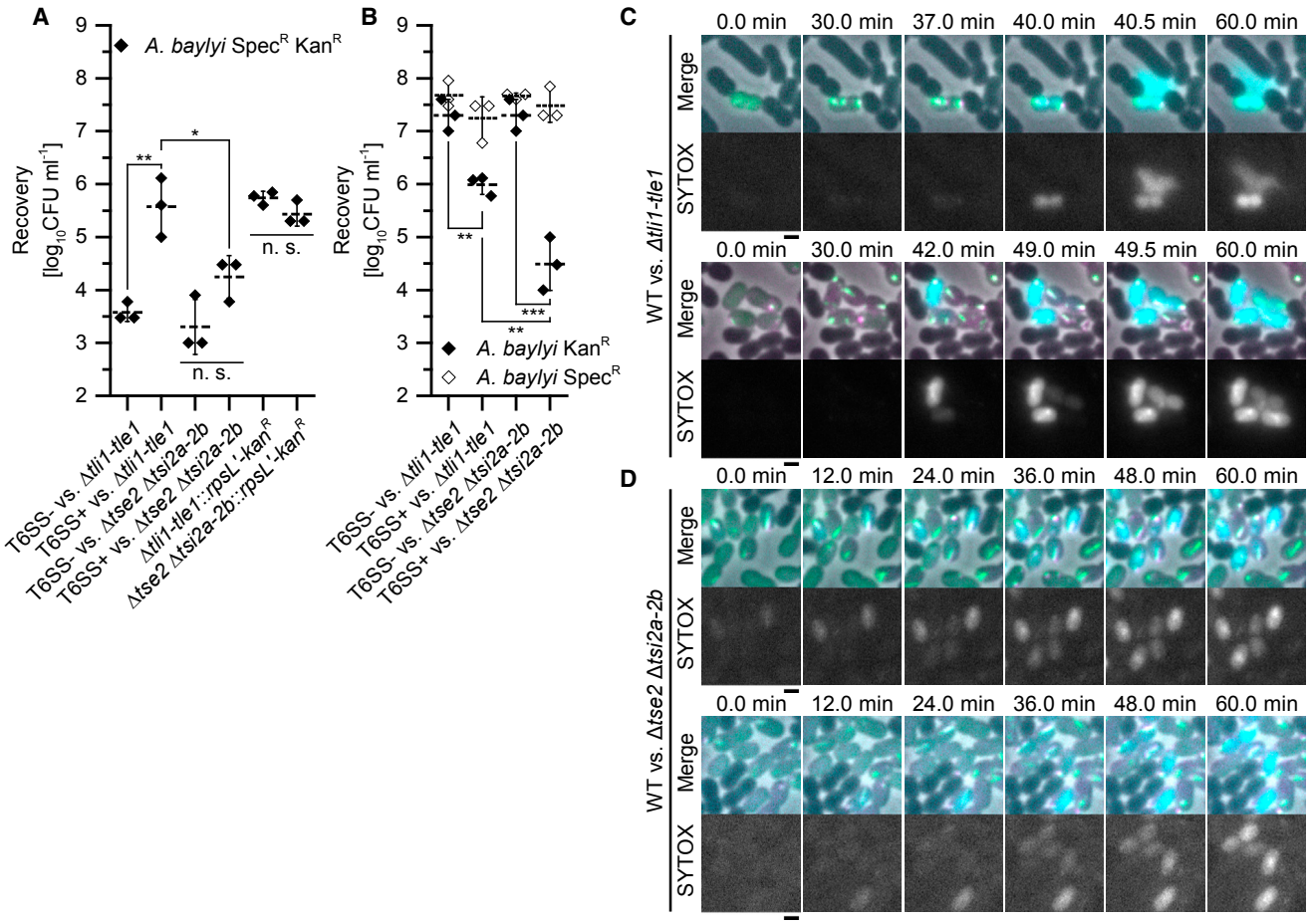

Figure 6. The Level of Horizontal Gene Transfer Depends on the Mechanism of Prey Cell Killing

(A) The level of DNA transfer between the indicated strains was tested by enumerating the clones having acquired a resistance cassette after 4 hr of coincubation. The control transformations of the T6SS$^+$ strain with genomic DNA are labeled as Δ*tli1-tle1*::*rpsL'-kan*^{R} and Δ*tse2* Δ*tsi2a-2b*::*rpsL'-kan*^{R}.

(B) Quantitative competition assay measuring the recovery of the indicated strains coincubated as in (A). The dashed lines indicate the means and the error bars indicate the SD. n. s. = not significant; *p < 0.05; **p < 0.01; *** p < 0.001.

(C and D) Time-lapse microscopy illustrating the distinct lysis phenotypes of the Δ*tli1-tle1* (C) and the Δ*tse2* Δ*tsi2a-2b* (D) sensitive strains (*vipA-sfGFP clpV-mcherry2* background) incubated with unlabeled wild-type *A. baylyi* ADP1. The top rows show a merge of phase contrast, GFP (green), mCherry (magenta), and SYTOX (cyan) channels. The bottom rows show the increase in the fluorescence of the cell-impermeable DNA stain SYTOX Blue upon the loss of cell membrane integrity. The mixtures were imaged every 30 s for 1 hr. The scale bars represent 1 μm.

diderm bacteria with an atomic force microscopy (AFM) tip does not affect their viability, which was explained by the "self-healing" capabilities of the cell envelope after AFM tip removal (Suo et al., 2009). On the other hand, R-type pyocins, which are structurally and mechanistically related to the T6SS, insert a tube into the target cell envelope, which results in ion leakage and cell killing (Ge et al., 2015; Michel-Briand and Baysse, 2002). This therefore suggests that the T6SS tube is likely unstable, and after delivery to the target cell, the Hcp tube dissociates, allowing the membranes to reseal.

All of the identified T6SS effectors (except Tpe1) were capable of significantly inhibiting or lysing *E. coli* (Figures 3A and 3C). Similarly, other bacteria carrying antibacterial effectors were often shown to deploy more than one antibacterial effector (Alcoforado Diniz et al., 2015). For example, *V. cholerae* has been demonstrated to utilize effector sets for intraspecific competition, where strains with incompatible combinations of effectors and immunity proteins will intoxicate one another (Unterweger et al., 2014). Interestingly, the T6SS of *V. cholerae* is involved in horizontal gene transfer (Borgeaud et al., 2015), and *V. cholerae* was also shown to be capable of acquiring new effector-immunity pairs or of exchanging old ones while retaining the corresponding immunity protein (Kirchberger et al., 2017; Unterweger et al., 2014). Similarly, the T6SS of the naturally competent *A. baylyi* ADP1 was recently shown to promote transfer of a plasmid from prey to predator (Cooper et al., 2017). The related *A. baumannii* strains, while not generally naturally competent under laboratory conditions, carry similar genes required to uptake DNA and kill target cells. It is therefore tempting to speculate that the T6SS-mediated killing of target cells by *A. baumannii* could be contributing to the highly efficient spread of drug resistance genes (Cooper et al., 2017), especially

Table 1. Summary of Knockout Phenotypes

Deletion	Competitor Inhibition	Hcp	Dynamics	Lysis	Previously Observed Phenotypes
tssE	0	0	+/0	0	approximately 1,000-fold less active in *V. cholerae* with no detectable competitor CFU reduction, but residual prey lysis (Vettiger and Basler, 2016)
tagF	+++	+++	+++	+++	increased Hcp secretion in *P. aeruginosa* (Silverman et al., 2011) and *B. cenocepacia* (Aubert et al., 2015)
tagN	++	+++	++	++	this study and Weber et al., 2016
tagX	0	0	+	+	this study and Weber et al., 2016
ACIAD2685	0	0	+	++	this study and Weber et al., 2016
ACIAD2693	++	++	++	+++	this study and Weber et al., 2016
ACIAD2698	+++	+++	+++	+++	this study and Weber et al., 2016

The phenotypes are given as qualitative values: +++, similar to wild-type; ++, attenuated; +, detectable; 0, not detectable.

if competence and T6SS would be co-regulated as in *V. cholerae* (Borgeaud et al., 2015). However, it is also important to mention that many organisms, including *Acinetobacter* and *Vibrio*, may secrete DNases in a T6SS-dependent and -independent manner, which could decrease the rate of horizontal gene transfer.

Overall, potentially all bacteria that encode an anti-bacterial T6SS and DNA uptake machinery could use their T6SS to acquire new genes. In addition to *Vibrio* and *Acinetobacter*, this could be relevant for *Campylobacter*, *Pseudomonas*, *Agrobacterium*, and *Ralstonia*. Members of these genera were predicted to harbor a T6SS (Li et al., 2015) and to be naturally competent (reviewed in Johnston et al., 2014). The targeted lysis and acquisition of genes from bacteria occupying a certain environmental niche may provide an advantage to the T6SS-positive bacteria since the target bacteria likely carry genes that evolved to enhance survival in the niche (Veening and Blokesch, 2017). Importantly, the rate of horizontal gene transfer mediated by T6SSs will vary for each prey-predator pair, because the frequency of DNA acquisition depends on the mode of target cell killing (Figure 6). This suggests that for efficient DNA acquisition from various prey cells, a diverse set of lytic effectors delivered by the predator may be beneficial, as certain prey cells may be immune to some of those effectors.

EXPERIMENTAL PROCEDURES

Bioinformatic analyses were carried out as described in the Supplemental Experimental Procedures.

Culturing of the Bacterial Strains

The strains were grown shaking at 200 rpm and 30°C or 37°C in LB broth or on LB agar (LA) plates (1.3% [w/v] agar). The media were supplemented with the appropriate antibiotics. For *E. coli* MG1655 Gm^R, 15 μg/mL gentamicin was added, for *A. baylyi* ADP1 *rpsL*-K88R derivatives, 50 μg/mL streptomycin was added, and for *A. baylyi* ADP1 strains carrying the positive/negative selection cassette, 50 μg/mL kanamycin was added. The strains carrying a spectinomycin resistance cassette were grown in the presence of 300 μg/mL spectinomycin. *P. aeruginosa* PAO1 was first grown on an LA plate overnight, and then an LB overnight culture supplemented with 20 μg/mL irgasan was started from the plate. The strains used in this study are listed in Table S1.

Construction of the Positive/Negative Selection Cassette

A positive/negative selection cassette was constructed based on the recessive streptomycin resistance conferred by the genomic *rpsL*-K88R mutation (Lederberg, 1951). The positive/negative selection cassette used in this study consists of a synthetic gene encoding the native RpsL of *A. baylyi* ADP1 (IDT) under the control of the native P_{rpsL} and the *aph(3′)-Ia* conferring kanamycin resistance under the control of the P_{bla} from the pRSFDuet-1 (Novagen). The cassette was assembled using overlap extension PCR. The synthetic gene encoding the native RpsL of *A. baylyi* ADP1 was designed such that most codons were exchanged by non-identical synonymous codons to avoid recombination with the genomic *rpsL*-K88R allele. This cassette was inserted into *vipA* and sequenced. Whenever the cassette was needed, it was amplified from the genomic DNA of this initial strain. The full sequence of the cassette is in Data S1.

Generation of Chromosomal *A. baylyi* ADP1 Mutants

A. baylyi ADP1 mutants were generated based on the methods described earlier (Metzgar et al., 2004) with the modifications outlined below. The homologous flanking regions were typically chosen to be between 500 and 800 bp in length. Primers were derived from the *A. baylyi* ADP1 genomic DNA sequence (NC_005966.1 obtained from NCBI). To transform DNA to *A. baylyi*, an overnight culture was washed with LB and diluted 1:50 or 1:20 into fresh LB. The culture was then regrown for 5 hr or 2 hr and 45 min, respectively, shaking at 30°C and 200 rpm. Thereafter, a few microliters of the agarose gel-purified DNA fragment bearing the desired mutation were added to the culture, which was kept shaking at 30°C and 200 rpm for ≥1 hr. Subsequently, cells from a 1-mL culture were plated on an LA plate supplemented with the appropriate antibiotic. When selecting for the loss of the counter-selectable cassette, 100 μg/ml streptomycin was used. The efficiency of the negative selection was routinely over 90%. After restreaking for single colonies, the success of the mutagenesis was assessed by colony PCR and subsequent sequencing. For mutants in which the target gene was disrupted by the insertion of the counter-selectable cassette, additional mutations in the disrupted gene were tolerated. PCRs for sequencing, cloning, and construction of deletion cassettes were either performed with the Q5 High-Fidelity DNA Polymerase (NEB) or with Herculase II (Agilent). Colony PCRs were performed with Taq DNA Polymerase (Sigma-Aldrich) or Q5 High-Fidelity DNA Polymerase. The mutations generated in this study are listed in Table S2.

Quantitative Competition Assays

The quantitative competition assays were performed in biological triplicates starting from three separate overnight cultures of the predator and prey strains. The *vipA-sfGFP*- and *clpV-mCherry2*-labeled parental strain served as the positive control, and the derived Δ*tssM* strain served as the negative control. After overnight cultivation, the cultures were washed once with LB to remove the antibiotic. Thereafter, the *A. baylyi* ADP1 strains were diluted 1:20, the *E. coli* MG1655 $Gent^R$ was diluted 1:100, *P. aeruginosa* PAO1 was

diluted 1:40, and *P. aeruginosa* PAO1 Δ*retS* was diluted 1:20 in 3 mL fresh LB. These cultures were incubated shaking at 200 rpm and 30°C for approximately 2 hr 40 min to reach an optical density at 600 nm (OD_{600nm}) of 0.6–1.4 and then pelleted at 20,000 × g for 2 min. The pellets were resuspended in fresh LB to reach an OD_{600nm} of approximately 10. The predator and prey strains were mixed at a ratio of 1:1, and 5 μL of the mixtures were spotted on a pre-dried LA plate. The spots were allowed to dry, and then the competition was carried out at 30°C for 4 hr. Thereafter, the spots were excised from the plate, and the bacteria were resuspended in 0.5 mL LB. These suspensions were 7× serially diluted 1:10 with LB, and 5 μL of each sample was spotted on both a prey- and a predator-selective plate. For streptomycin-resistant *A. baylyi* ADP1 derivatives, 100 μg/mL streptomycin was used. For the other strains, the usual antibiotic concentrations were used. These plates were incubated at room temperature (RT) or 30°C until colonies were visible. For the comparisons, one-way ANOVA ($\alpha = 0.05$) with a subsequent Tukey post hoc test was performed using OriginPro 2016G.

Horizontal Gene Transfer Assay

The horizontal gene transfer assay was carried out as described for the quantitative competition assay, except that the serial dilutions of the recovered bacteria were spotted on three LA plates supplemented with 300 μg/mL spectinomycin, 50 μg/mL kanamycin, and both 300 μg/mL spectinomycin and 50 μg/mL kanamycin. For the control transformations, 203 ng of the prey strain genomic DNA was added to the concentrated predator instead of the concentrated prey strains. Thereafter, the assay was carried out as described for testing horizontal gene transfer between two strains.

Hcp Secretion Assay

For the Hcp secretion assay the *A. baylyi* ADP1 derivatives were regrown as described for the quantitative competition assay. Thereafter, 1 mL of the cultures were centrifuged for 1 min at 10,000 × g and 4°C. A total of 100 μL ice-cold 100% trichloroacetic acid (w/v; Sigma-Aldrich) was added to 900 μL of the supernatants, incubated on ice for 10 min with intermittent vortexing and then centrifuged for 5 min at 14,000 × g and 4°C. The pellets were washed with ice-cold acetone, dried at RT, and then resuspended in 20 μL 1× NuPAGE LDS sample buffer (Thermo Fisher Scientific); 2.22 μL 1 M dithiothreitol was added and then incubated at 70°C for 10 min. Three-quarters of these samples were loaded onto NuPAGE 4%–12% Bis-Tris 1.0-mm, 12-well protein gels (Thermo Fisher Scientific), which were run in MES buffer (Thermo Fisher Scientific) for 35 min at 200 V. The gels were stained with InstantBlue Coomassie protein stain (Expedeon) overnight and then destained with distilled water. The assay was performed in biological duplicate. The whole gels are shown in Figure S4.

Lysis Assay

The lysis assay is based on the chromogenic hydrolysis of the cell-impermeable β-galactosidase substrate chlorophenol red-β-D-galactopyranoside (CPRG; Sigma-Aldrich) (Vettiger and Basler, 2016) upon lysis of *E. coli* MG1655 $Gent^R$. The assay was carried out similarly to the quantitative competition assay described above, except that *E. coli* was regrown in the presence of 100 μM isopropyl-β-D-thiogalactoside (IPTG) to pre-induce the β-galactosidase. After pelleting, the *E. coli* pellet was resuspended in LB supplemented with 100 μM IPTG. Only 3 μL of the competition mixtures were spotted on 150 μL LA supplemented with 100 μM IPTG and 20 μg/mL CPRG in a flat-bottom 96-well plate in hexaplicate, leaving out the outer most wells. The spots were allowed to dry. Thereafter, the plate was incubated at 30°C without a lid in an Epoch 2 plate reader (BioTek) for 4 hr while measuring the absorption at 572 nm every 10 min. When the measurement was finished, a picture of a representative plate was taken. The SDs of the biological triplicates were calculated from the averages of the technical hexaplicates except where noted otherwise.

Fluorescence Microscopy

For imaging the T6SS dynamics of the *A. baylyi* ADP1 mutants and the competition microscopy, the strains were regrown, concentrated, and mixed, when appropriate, as described for the quantitative competition assay. The concentrated culture or mixture was spotted on a thin pad of 1% (w/v) agarose in LB, covered with a glass coverslip, and imaged. For the competition microscopy, the pad was supplemented with 0.5 μM SYTOX Blue Nucleic Acid Stain (Thermo Fisher Scientific). The microscopic imaging was performed at least in biological duplicate.

The following setup was used for microscopy: a Nikon Ti-E inverted motorized microscope with Perfect Focus System and Plan Apo 100× Oil Ph3 DM (NA, 1.4) objective lens, SPECTRA X light engine (Lumencor) and ET-ECFP (Chroma #49001), ET-GFP (Chroma #49002), and ET-mCherry (Chroma #49008) filter set. A pco.edge 4.2 (PCO, Germany) scientific complementary metal-oxide-semiconductor (sCMOS) camera (pixel size, 65 nm) and VisiView software (Visitron Systems, Germany) were used to record the images. The power output of the SPECTRA X light engine was set to 20% for all excitation wavelengths. The sfGFP and SYTOX Blue images were acquired with 100-ms exposure, whereas the mCherry2 images were acquired with 200-ms exposure. A climate chamber mounted around the stage and a heating collar around the objective were used to perform the imaging at 30°C and 95% relative humidity (R. H.). The obtained images were post-processed with Fiji (Schindelin et al., 2012) and custom software based on StackReg (Thévenaz et al., 1998). The contrast settings were adjusted such that the whole display range was used for the bright field channel (0–65535). For the other channels, the minimal value was set as the lower bound, and the upper bound was set to allow 5% of the pixels to saturate. The same contrast settings were used for each frame of a time lapse.

Statistical Analysis

The number of biological replicates is indicated for each experiment. When measuring the colony forming units (CFUs) per milliliter, first the decadic logarithm was taken, and then the averages and SDs were calculated from the transformed values. For the comparisons, one-way ANOVA ($\alpha = 0.05$) with a Tukey post hoc test was performed using OriginPro 2016G. For the CPRG assays, the averages and the SDs of the biological replicates were calculated from the averages of the technical replicates.

SUPPLEMENTAL INFORMATION

Supplemental Information includes Supplemental Experimental Procedures, four figures, two tables, three movies, and one data file and can be found with this article online at https://doi.org/10.1016/j.celrep.2017.12.020.

ACKNOWLEDGMENTS

This work was supported by Swiss National Science Foundation Starting Grant BSSGI0_155778 and the University of Basel. P.D.R. was supported by the Biozentrum Basel International Ph.D. Program, Fellowships for Excellence.

AUTHOR CONTRIBUTIONS

Conceptualization, M.B. and P.D.R.; Methodology, M.B., D.H., and P.D.R.; Investigation, D.H. and P.D.R.; Writing – Original Draft, M.B. and P.D.R.; Writing – Review & Editing, M.B. and P.D.R.; Funding Acquisition, M.B.; Resources, M.B.; Supervision, M.B.

DECLARATION OF INTERESTS

The authors declare no competing interests.

Received: August 25, 2017
Revised: November 22, 2017
Accepted: December 5, 2017
Published: December 26, 2017

REFERENCES

Alcoforado Diniz, J., Liu, Y.-C., and Coulthurst, S.J. (2015). Molecular weaponry: diverse effectors delivered by the Type VI secretion system. Cell. Microbiol. *17*, 1742–1751.

Aschtgen, M.-S., Thomas, M.S., and Cascales, E. (2010). Anchoring the type VI secretion system to the peptidoglycan: TssL, TagL, TagP… what else? Virulence *1*, 535–540.

Aubert, D.F., Hu, S., and Valvano, M.A. (2015). Quantification of type VI secretion system activity in macrophages infected with *Burkholderia cenocepacia*. Microbiology *161*, 2161–2173.

Basler, M., and Mekalanos, J.J. (2012). Type 6 secretion dynamics within and between bacterial cells. Science *337*, 815.

Basler, M., Pilhofer, M., Henderson, G.P., Jensen, G.J., and Mekalanos, J.J. (2012). Type VI secretion requires a dynamic contractile phage tail-like structure. Nature *483*, 182–186.

Basler, M., Ho, B.T., and Mekalanos, J.J. (2013). Tit-for-tat: type VI secretion system counterattack during bacterial cell-cell interactions. Cell *152*, 884–894.

Bingle, L.E., Bailey, C.M., and Pallen, M.J. (2008). Type VI secretion: a beginner's guide. Curr. Opin. Microbiol. *11*, 3–8.

Böck, D., Medeiros, J.M., Tsao, H.-F., Penz, T., Weiss, G.L., Aistleitner, K., Horn, M., and Pilhofer, M. (2017). In situ architecture, function, and evolution of a contractile injection system. Science *357*, 713–717.

Bondage, D.D., Lin, J.-S., Ma, L.-S., Kuo, C.-H., and Lai, E.-M. (2016). VgrG C terminus confers the type VI effector transport specificity and is required for binding with PAAR and adaptor-effector complex. Proc. Natl. Acad. Sci. USA *113*, E3931–E3940.

Bönemann, G., Pietrosiuk, A., Diemand, A., Zentgraf, H., and Mogk, A. (2009). Remodelling of VipA/VipB tubules by ClpV-mediated threading is crucial for type VI protein secretion. EMBO J. *28*, 315–325.

Borgeaud, S., Metzger, L.C., Scrignari, T., and Blokesch, M. (2015). The type VI secretion system of *Vibrio cholerae* fosters horizontal gene transfer. Science *347*, 63–67.

Brodmann, M., Dreier, R.F., Broz, P., and Basler, M. (2017). *Francisella* requires dynamic type VI secretion system and ClpB to deliver effectors for phagosomal escape. Nat. Commun. *8*, 15853.

Brunet, Y.R., Zoued, A., Boyer, F., Douzi, B., and Cascales, E. (2015). The type VI secretion TssEFGK-VgrG phage-like baseplate is recruited to the TssJLM membrane complex via multiple contacts and serves as assembly platform for tail tube/sheath polymerization. PLoS Genet. *11*, e1005545.

Chang, Y.-W., Rettberg, L.A., Ortega, D.R., and Jensen, G.J. (2017). In vivo structures of an intact type VI secretion system revealed by electron cryotomography. EMBO Rep. *18*, 1090–1099.

Clemens, D.L., Ge, P., Lee, B.-Y., Horwitz, M.A., and Zhou, Z.H. (2015). Atomic structure of T6SS reveals interlaced array essential to function. Cell *160*, 940–951.

Cooper, R.M., Tsimring, L., and Hasty, J. (2017). Inter-species population dynamics enhance microbial horizontal gene transfer and spread of antibiotic resistance. eLife *6*, e25950.

Costa, T.R.D., Felisberto-Rodrigues, C., Meir, A., Prevost, M.S., Redzej, A., Trokter, M., and Waksman, G. (2015). Secretion systems in Gram-negative bacteria: structural and mechanistic insights. Nat. Rev. Microbiol. *13*, 343–359.

de Bruin, O.M., Ludu, J.S., and Nano, F.E. (2007). The *Francisella* pathogenicity island protein IglA localizes to the bacterial cytoplasm and is needed for intracellular growth. BMC Microbiol. *7*, 1.

Dong, T.G., Ho, B.T., Yoder-Himes, D.R., and Mekalanos, J.J. (2013). Identification of T6SS-dependent effector and immunity proteins by Tn-seq in *Vibrio cholerae*. Proc. Natl. Acad. Sci. USA *110*, 2623–2628.

Durand, E., Nguyen, V.S., Zoued, A., Logger, L., Péhau-Arnaudet, G., Aschtgen, M.-S., Spinelli, S., Desmyter, A., Bardiaux, B., Dujeancourt, A., et al. (2015). Biogenesis and structure of a type VI secretion membrane core complex. Nature *523*, 555–560.

Ge, P., Scholl, D., Leiman, P.G., Yu, X., Miller, J.F., and Zhou, Z.H. (2015). Atomic structures of a bactericidal contractile nanotube in its pre- and post-contraction states. Nat. Struct. Mol. Biol. *22*, 377–382.

Hachani, A., Allsopp, L.P., Oduko, Y., and Filloux, A. (2014). The VgrG proteins are "à la carte" delivery systems for bacterial type VI effectors. J. Biol. Chem. *289*, 17872–17884.

Ho, B.T., Basler, M., and Mekalanos, J.J. (2013). Type 6 secretion system-mediated immunity to type 4 secretion system-mediated gene transfer. Science *342*, 250–253.

Jiang, F., Waterfield, N.R., Yang, J., Yang, G., and Jin, Q. (2014). A *Pseudomonas aeruginosa* type VI secretion phospholipase D effector targets both prokaryotic and eukaryotic cells. Cell Host Microbe *15*, 600–610.

Johnston, C., Martin, B., Fichant, G., Polard, P., and Claverys, J.-P. (2014). Bacterial transformation: distribution, shared mechanisms and divergent control. Nat. Rev. Microbiol. *12*, 181–196.

Kirchberger, P.C., Unterweger, D., Provenzano, D., Pukatzki, S., and Boucher, Y. (2017). Sequential displacement of Type VI Secretion System effector genes leads to evolution of diverse immunity gene arrays in *Vibrio cholerae*. Sci. Rep. *7*, 45133.

Kudryashev, M., Wang, R.Y.-R., Brackmann, M., Scherer, S., Maier, T., Baker, D., DiMaio, F., Stahlberg, H., Egelman, E.H., and Basler, M. (2015). Structure of the type VI secretion system contractile sheath. Cell *160*, 952–962.

Lederberg, J. (1951). Streptomycin resistance; a genetically recessive mutation. J. Bacteriol. *61*, 549–550.

Leong, C.G., Boyd, C.M., Roush, K.S., Tenente, R., Lang, K.M., and Lostroh, C.P. (2017). Succinate, iron chelation, and monovalent cations affect the transformation efficiency of *Acinetobacter baylyi* ATCC 33305 during growth in complex media. Can. J. Microbiol. *63*, 851–856.

Li, J., Yao, Y., Xu, H.H., Hao, L., Deng, Z., Rajakumar, K., and Ou, H.-Y. (2015). SecReT6: a web-based resource for type VI secretion systems found in bacteria. Environ. Microbiol. *17*, 2196–2202.

Liang, X., Moore, R., Wilton, M., Wong, M.J.Q., Lam, L., and Dong, T.G. (2015). Identification of divergent type VI secretion effectors using a conserved chaperone domain. Proc. Natl. Acad. Sci. USA *112*, 9106–9111.

Ma, J., Pan, Z., Huang, J., Sun, M., Lu, C., and Yao, H. (2017). The Hcp proteins fused with diverse extended-toxin domains represent a novel pattern of antibacterial effectors in type VI secretion systems. Virulence *8*, 1189–1202.

Metzgar, D., Bacher, J.M., Pezo, V., Reader, J., Döring, V., Schimmel, P., Marlière, P., and de Crécy-Lagard, V. (2004). *Acinetobacter* sp. ADP1: an ideal model organism for genetic analysis and genome engineering. Nucleic Acids Res. *32*, 5780–5790.

Michel-Briand, Y., and Baysse, C. (2002). The pyocins of *Pseudomonas aeruginosa*. Biochimie *84*, 499–510.

Planamente, S., Salih, O., Manoli, E., Albesa-Jové, D., Freemont, P.S., and Filloux, A. (2016). TssA forms a gp6-like ring attached to the type VI secretion sheath. EMBO J. *35*, 1613–1627.

Pukatzki, S., Ma, A.T., Sturtevant, D., Krastins, B., Sarracino, D., Nelson, W.C., Heidelberg, J.F., and Mekalanos, J.J. (2006). Identification of a conserved bacterial protein secretion system in *Vibrio cholerae* using the *Dictyostelium* host model system. Proc. Natl. Acad. Sci. USA *103*, 1528–1533.

Pukatzki, S., Ma, A.T., Revel, A.T., Sturtevant, D., and Mekalanos, J.J. (2007). Type VI secretion system translocates a phage tail spike-like protein into target cells where it cross-links actin. Proc. Natl. Acad. Sci. USA *104*, 15508–15513.

Russell, A.B., Singh, P., Brittnacher, M., Bui, N.K., Hood, R.D., Carl, M.A., Agnello, D.M., Schwarz, S., Goodlett, D.R., Vollmer, W., and Mougous, J.D. (2012). A widespread bacterial type VI secretion effector superfamily identified using a heuristic approach. Cell Host Microbe *11*, 538–549.

Russell, A.B., LeRoux, M., Hathazi, K., Agnello, D.M., Ishikawa, T., Wiggins, P.A., Wai, S.N., and Mougous, J.D. (2013). Diverse type VI secretion phospholipases are functionally plastic antibacterial effectors. Nature *496*, 508–512.

Russell, A.B., Wexler, A.G., Harding, B.N., Whitney, J.C., Bohn, A.J., Goo, Y.A., Tran, B.Q., Barry, N.A., Zheng, H., Peterson, S.B., et al. (2014a). A type VI secretion-related pathway in *Bacteroidetes* mediates interbacterial antagonism. Cell Host Microbe *16*, 227–236.

Russell, A.B., Peterson, S.B., and Mougous, J.D. (2014b). Type VI secretion system effectors: poisons with a purpose. Nat. Rev. Microbiol. *12*, 137–148.

Santin, Y.G., and Cascales, E. (2017). Domestication of a housekeeping transglycosylase for assembly of a Type VI secretion system. EMBO Rep. *18*, 138–149.

Schindelin, J., Arganda-Carreras, I., Frise, E., Kaynig, V., Longair, M., Pietzsch, T., Preibisch, S., Rueden, C., Saalfeld, S., Schmid, B., et al. (2012). Fiji: an open-source platform for biological-image analysis. Nat. Methods *9*, 676–682.

Shneider, M.M., Buth, S.A., Ho, B.T., Basler, M., Mekalanos, J.J., and Leiman, P.G. (2013). PAAR-repeat proteins sharpen and diversify the type VI secretion system spike. Nature *500*, 350–353.

Silverman, J.M., Austin, L.S., Hsu, F., Hicks, K.G., Hood, R.D., and Mougous, J.D. (2011). Separate inputs modulate phosphorylation-dependent and -independent type VI secretion activation. Mol. Microbiol. *82*, 1277–1290.

Silverman, J.M., Agnello, D.M., Zheng, H., Andrews, B.T., Li, M., Catalano, C.E., Gonen, T., and Mougous, J.D. (2013). Haemolysin coregulated protein is an exported receptor and chaperone of type VI secretion substrates. Mol. Cell *51*, 584–593.

Suo, Z., Avci, R., Deliorman, M., Yang, X., and Pascual, D.W. (2009). Bacteria survive multiple puncturings of their cell walls. Langmuir *25*, 4588–4594.

Taylor, N.M.I., Prokhorov, N.S., Guerrero-Ferreira, R.C., Shneider, M.M., Browning, C., Goldie, K.N., Stahlberg, H., and Leiman, P.G. (2016). Structure of the T4 baseplate and its function in triggering sheath contraction. Nature *533*, 346–352.

The UniProt Consortium (2017). UniProt: the universal protein knowledgebase. Nucleic Acids Res. *45* (*D1*), D158–D169.

Thévenaz, P., Ruttimann, U.E., and Unser, M. (1998). A pyramid approach to subpixel registration based on intensity. IEEE Trans. Image Process. *7*, 27–41.

Unterweger, D., Miyata, S.T., Bachmann, V., Brooks, T.M., Mullins, T., Kostiuk, B., Provenzano, D., and Pukatzki, S. (2014). The *Vibrio cholerae* type VI secretion system employs diverse effector modules for intraspecific competition. Nat. Commun. *5*, 3549.

Unterweger, D., Kostiuk, B., Ötjengerdes, R., Wilton, A., Diaz-Satizabal, L., and Pukatzki, S. (2015). Chimeric adaptor proteins translocate diverse type VI secretion system effectors in *Vibrio cholerae*. EMBO J. *34*, 2198–2210.

Veening, J.-W., and Blokesch, M. (2017). Interbacterial predation as a strategy for DNA acquisition in naturally competent bacteria. Nat. Rev. Microbiol. *15*, 621–629.

Vettiger, A., and Basler, M. (2016). Type VI secretion system substrates are transferred and reused among sister cells. Cell *167*, 99–110.e12.

Vettiger, A., Winter, J., Lin, L., and Basler, M. (2017). The type VI secretion system sheath assembles at the end distal from the membrane anchor. Nat. Commun. *8*, 16088.

Wang, J., Brackmann, M., Castaño-Díez, D., Kudryashev, M., Goldie, K.N., Maier, T., Stahlberg, H., and Basler, M. (2017). Cryo-EM structure of the extended type VI secretion system sheath-tube complex. Nat. Microbiol. *2*, 1507–1512.

Weber, B.S., Miyata, S.T., Iwashkiw, J.A., Mortensen, B.L., Skaar, E.P., Pukatzki, S., and Feldman, M.F. (2013). Genomic and functional analysis of the type VI secretion system in *Acinetobacter*. PLoS ONE *8*, e55142.

Weber, B.S., Hennon, S.W., Wright, M.S., Scott, N.E., de Berardinis, V., Foster, L.J., Ayala, J.A., Adams, M.D., and Feldman, M.F. (2016). Genetic dissection of the type VI secretion system in *Acinetobacter* and identification of a novel peptidoglycan hydrolase, TagX, required for its biogenesis. MBio *7*, e01253–e16.

Wilton, M., Wong, M.J.Q., Tang, L., Liang, X., Moore, R., Parkins, M.D., Lewenza, S., and Dong, T.G. (2016). Chelation of membrane-bound cations by extracellular DNA activates the type VI secretion system in *Pseudomonas aeruginosa*. Infect. Immun. *84*, 2355–2361.

Zhang, D., de Souza, R.F., Anantharaman, V., Iyer, L.M., and Aravind, L. (2012). Polymorphic toxin systems: Comprehensive characterization of trafficking modes, processing, mechanisms of action, immunity and ecology using comparative genomics. Biol. Direct *7*, 18.

Zoued, A., Durand, E., Brunet, Y.R., Spinelli, S., Douzi, B., Guzzo, M., Flaugnatti, N., Legrand, P., Journet, L., Fronzes, R., et al. (2016). Priming and polymerization of a bacterial contractile tail structure. Nature *531*, 59–63.